This article has been accepted for inclusion in a future issue of this journal. Content is final as presented, with the exception of pagination.

MPC-Based Energy Management of a Power-Split Hybrid Electric Vehicle

Hoseinali Borhan, *Student Member, IEEE*, Ardalan Vahidi, *Member, IEEE*, Anthony M. Phillips, Ming L. Kuang, Ilya V. Kolmanovsky, *Fellow, IEEE*, and Stefano Di Cairano, *Member, IEEE*

***Abstract*—A power-split hybrid electric vehicle (HEV) combines the advantages of both series and parallel hybrid vehicle architectures by utilizing a planetary gear set to split and combine the power produced by electric machines and a combustion engine. Because of the different modes of operation, devising a near optimal energy management strategy is quite challenging and essential for these vehicles. To improve the fuel economy of a power-split HEV, we first formulate the energy management problem as a nonlinear and constrained optimal control problem. Then two different cost functions are defined and model predictive control (MPC) strategies are utilized to obtain the power split between the combustion engine and electrical machines and the system operating points at each sample time. Simulation results on a closed-loop high-fidelity model of a power-split HEV over multiple standard drive cycles and with different controllers are presented. The results of a nonlinear MPC strategy show a noticeable improvement in fuel economy with respect to those of an available controller in the commercial Powertrain System Analysis Toolkit (PSAT) software and the other proposed methodology by the authors based on a linear time-varying MPC.**

***Index Terms*—Energy management, hybrid electric vehicle (HEV), linear time-varying model predictive control (LTV-MPC), MPC, nonlinear MPC, power-split HEV.**

I. Introduction

HYBRID electric vehicles (HEVs) provide improved fuel economy due to extra degree(s) of freedom provided by battery energy storage and one or more electric machine(s) which allow running a smaller combustion engine in a higher efficiency region [1]. The battery storage also enables capturing the braking energy, which is wasted as heat in conventional vehicles. Among possible configurations of a hybrid electric powertrain, power-split, or parallel-series which provides both series and parallel functionality are produced by several auto-makers. The Ford Escape Hybrid and Toyota Prius both have a power-split powertrain. Fig. 1 shows a schematic view of a power-split HEV which is discussed in this research. In this configuration, the engine and the generator are connected to the planet carrier and sun gear of a planetary gear set or speed coupler, respectively. The output of the speed coupler is combined with a second motor/generator through a torque coupler to power the vehicle driveline. Because of the different possible power flows in the power-split powertrain, the engine operating point can be seen as decoupled from the vehicle operating point. In addition, the battery storage system provides another degree of freedom to accumulate or deliver energy. Thus, there are two degrees-of-freedom for the energy management of these HEVs that together with the different modes of operation allow the vehicle to operate more efficiently and consequently to achieve reduced fuel consumption and emissions.

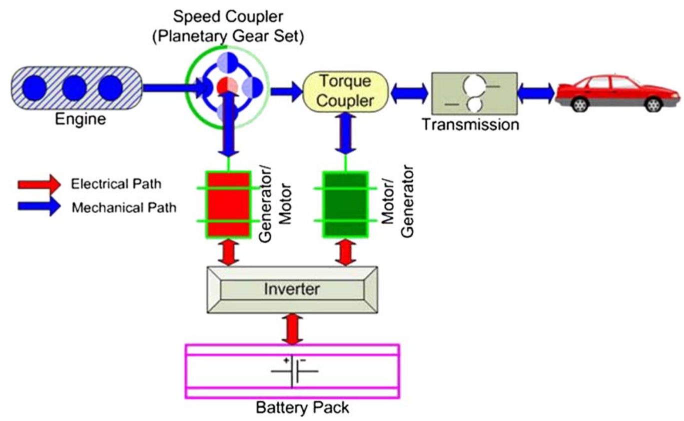

Fig. 1. Power-split HEV configuration.

Improvement of fuel economy in HEVs strongly depends on the employed energy management strategy. When formulated in an optimal control framework, the energy management problem becomes a nonlinear, constrained, and dynamic optimization problem, due to the nonlinearities of the dynamic model of the powertrain and several equality and inequality constraints on the states and on the control inputs. In the past, researchers have used numerical solutions, e.g., based on dynamic programming (DP) [2], [3] or have simplified the dynamic optimization problem to an equivalent instantaneous optimization, called equivalent consumption minimization strategy (ECMS) [4]–[6]. Comprehensive reviews of these optimal control methods, along with heuristic rule-based methods, can be found in [6] and [7]. If we assume to have the full knowledge of the future driving conditions, the globally optimal solution for a model of the HEV can be derived using dynamic programming. However, the DP

Manuscript received May 13, 2010; revised December 17, 2010; accepted February 07, 2011. Manuscript received in final form March 22, 2011. Recommended by Associate Editor J. H. Lee. This work was supported by a University Research Program (URP) Grant from Ford Motor Company.

H. Borhan and A. Vahidi are with the Department of Mechanical Engineering, Clemson University, Clemson, SC 29634 USA (e-mail: hborhan@clemson.edu; avahidi@clemson.edu).

A. M. Phillips, M. L. Kuang, and S. Di Cairano are with Ford Research and Advanced Engineering, Dearborn, MI 48121 USA (e-mail: aphilli8@ford.com; mkuang@ford.com; sdicaira@ford.com).

I. V. Kolmanovsky is with the Department of Aerospace Engineering, University of Michigan, Ann Arbor, MI 48109 USA (e-mail: ilya@umich.edu).

Color versions of one or more of the figures in this paper are available online at http://ieeexplore.ieee.org.

Digital Object Identifier 10.1109/TCST.2011.2134852

solution is non-causal due to its dependence on unknown future power demand, and it is computationally demanding when a long horizon is considered. The DP solutions over the known driving cycles have been used mainly as benchmarks for the best achievable fuel economy [8]. By defining an equivalent fuel cost for the battery energy, ECMS methods have been developed to be solved at each instant rather than over the driving interval [4], [5], [9]. Although ECMS can be applied online as a closed-loop controller, the decisions are non-predictive because the dynamics of the system (battery in general) are not considered. A compromise between the computational cost and the non-causality of a globally optimal DP solution and the faster, causal, but instantaneous ECMS solution can be formed in an energy management strategy based on the model predictive control (MPC), where the optimization is performed over a moving finite horizon.

Starting from the initial investigation in [10], we develop a linear time-varying MPC (LTV-MPC) [11] with a quadratic cost function for the energy management problem. The LTV-MPC results are comparable with a well-tuned controller of PSAT software [12], yet further improvement in the fuel economy was desirable. Thus, we reformulate the MPC fuel minimization problem to include not only the fuel cost over a finite horizon but also an approximate cost-to-go beyond the planning horizon represented as a terminal cost in the MPC. We use the relationship between the Hamilton-Jacobi-Bellman (HJB) equation and the Pontryagin's minimum principle [13] to show that the cost-to-go for this optimal control problem can be approximated as a piecewise linear function of the deviations in the battery state of charge. Our derivations are in accordance with the results in [14] developed in parallel to our research. A nonlinear MPC framework is employed to solve the optimal control problem online. Simulation results on a closed-loop model of a power-split HEV with respect to both the LTV-MPC and the PSAT software show noticeable improvements.

This paper is organized as follows. The model of the power-split HEV is first presented and its constraints are discussed in Section II where a control-oriented model for the design of the MPC controllers is derived. The control system structure and the fuel minimization problem are presented in Section III. In Section IV, the energy management strategy based on a linear time-varying MPC is formulated using a quadratic cost function. The results of the LTV-MPC over a high-fidelity closed-loop model of a power-split HEV are presented in this section. In Section V, a different cost functional is derived and the optimal control problem is reformulated. Using a nonlinear MPC framework, an energy management strategy is developed and its results are presented and compared with the ones of LTV-MPC controller and the base controller of the PSAT software.

II. Plant Model

In this paper, for the closed-loop simulations we use a detailed model of a power-split HEV from the database of Powertrain Simulation Analysis Toolkit (PSAT) commercial software [12]. PSAT is a state-of-the-art flexible powertrain simulation software developed by Argonne National Laboratory with the support of automotive manufacturers and sponsored by the U.S. Department of Energy (DOE). It runs in a MATLAB/Simulink environment and provides access to dynamic models of different mechanical and electrical components of several hybrid vehicle configurations. The level of details in PSAT component models and its forward simulation approach ensures reliable estimation of the fuel economy. The modeling accuracy of PSAT has been validated against production HEVs such as the Honda Insight [15] and the Toyota Prius [16]. In order to analyze the performance of our MPC energy management strategies on a high-fidelity dynamic model of a power-split HEV, the PSAT Simulink model of the Toyota Prius was chosen as the plant model for the closed-loop simulations. The MPC module receives all of its feedback signals from the PSAT model and applies the engine torque and speed commands to the model. Because the PSAT model is too complex for control design, a simplified control-oriented model that captures the details that are of importance for the supervisory energy management system is derived in this section. Fig. 1 shows the main components of a power-split HEV which are modeled for designing the MPC-based supervisory controllers. More modeling details are available in [10], [17], and [18].

The battery's state of charge SOC is the main state in optimal control of HEV's as explained in [8] and its dynamics can be represented by

$$\frac{d\mathrm{SOC}}{dt} = -\frac{V_{oc} - \sqrt{V_{oc}^2 - 4P_{\mathrm{batt}}R_{\mathrm{batt}}}}{2C_{\mathrm{batt}}R_{\mathrm{batt}}} \tag{1}$$

where

$$P_{\mathrm{batt}} = P_{\mathrm{mot}} + P_{\mathrm{gen}} + P_{\mathrm{motor}}^{\mathrm{loss}} + P_{\mathrm{gen}}^{\mathrm{loss}}. \tag{2}$$

In (1) and (2), V_{oc}, R_{batt}, and C_{batt} are the battery open-circuit voltage, internal resistance, and capacity, respectively; P_{batt} is the battery power; P_{mot} and P_{gen} are the motor and generator power, respectively; and $P_{\mathrm{motor}}^{\mathrm{loss}}$ and $P_{\mathrm{gen}}^{\mathrm{loss}}$ are the motor and generator power losses, respectively. In (1), positive battery power $(P_{\mathrm{batt}} > 0)$ indicates the battery is discharging and negative battery power $(P_{\mathrm{batt}} < 0)$ indicates battery is charging. Empirical maps, extracted from PSAT, are used to calculate the power losses of the motor and generator as functions of the corresponding torque and speed.

The power-split powertrain, also called the electric-continuously variable transmission, includes a planetary gear set (speed coupler) which combines the power of the engine, motor, and generator. This power coupling can be accomplished such that the engine operating point becomes independent of the vehicle operation. Neglecting the inertia of pinion gears in the planetary gear set and assuming that all the connecting shafts in the powertrain are rigid, the inertial dynamics of the powertrain can be obtained using Newton's laws [10]

$$\begin{aligned} J_{\mathrm{gen}}\frac{d\omega_{\mathrm{gen}}}{dt} &= T_{\mathrm{gen}} + F \times N_S \\ J_{\mathrm{eng}}\frac{d\omega_{\mathrm{eng}}}{dt} &= T_{\mathrm{eng}} - F \times (N_S + N_R) \\ J_{\mathrm{mot}}\frac{d\omega_{\mathrm{mot}}}{dt} &= T_{\mathrm{mot}} - \frac{T_{\mathrm{out}}}{g_f} + F \times N_R \end{aligned} \tag{3}$$

where J_{gen} is the lumped inertia of the generator and the carrier gear; J_{eng} is the lumped inertia of the engine and the sun gear;

and J_{mot} is the inertia of the motor lumped with the inertias of the ring, final transmission, and wheels. In (3), N_S and N_R are the radii of the sun and ring gears; T_{eng}, T_{gen}, and T_{mot} are the engine, generator, and motor torques, respectively; ω_{eng}, ω_{gen}, and ω_{mot} are the engine, generator, and motor speeds, respectively; and T_{out} is the output torque of the powertrain. Finally in (3), F is the interaction force between the different gears. To reduce the number of dynamic states, the inertial losses of the engine, motor, and generator, i.e., $J_{\mathrm{eng}}(d\omega_{\mathrm{eng}}/dt)$, $J_{\mathrm{mot}}(d\omega_{\mathrm{mot}}/dt)$, and $J_{\mathrm{gen}}(d\omega_{\mathrm{gen}}/dt)$, are ignored and set to zero in the control-oriented model, a reasonable assumption since the rotational dynamics are much faster than the battery dynamics (1) and the inertial losses are limited. As a result, the relationships in (3) are reduced to three static equality constraints. An empirical map of the engine, extracted from PSAT software, is used to relate the fuel flow rate, $\dot{m}_f$, to the engine speed and torque as

$$\dot{m}_f = \varphi(\omega_{\mathrm{eng}}, \tau_{\mathrm{eng}}). \tag{4}$$

There are also two kinematic equality constraints between velocities

$$N_s\omega_{\mathrm{gen}} + N_R\omega_{\mathrm{mot}} = (N_s + N_R)\omega_{\mathrm{eng}} \tag{5}$$
$$\omega_{\mathrm{mot}} = \frac{g_f}{r_w}V \tag{6}$$

where V is the vehicle velocity with the following dynamics:

$$m\frac{dV}{dt} = \frac{T_{\mathrm{out}} + T_b}{r_w} - \frac{1}{2}\rho A_f C_d V^2 - C_r mg\cos(\theta) + mg\sin(\theta). \tag{7}$$

In (6) and (7), g_f is the final transmission gear ratio; m and A_f are the mass and frontal area of the vehicle, respectively; r_w is the wheel radius; C_r is the rolling resistance coefficient; C_d and ρ are the drag coefficient and air density, respectively; θ is the road grade which is assumed to be positive when vehicle is driven down a hill; and g is the gravity acceleration. The driveability constraint requires that the total torque at the wheels, which is the sum of the powertrain output torque T_{out} and the friction brake torque[1] T_b, is equal to the driver demanded torque T_{driver}

$$T_{\mathrm{out}} + T_b = T_{\mathrm{driver}}. \tag{8}$$

Assuming the driveability constraint (8) holds and using the vehicle speed dynamics (7), the vehicle velocity profile along a prediction horizon can be uniquely determined for an initial velocity and a driver torque profile. Furthermore, the following physical constraints, usually time-varying, must be enforced:

$$\begin{aligned} \mathrm{SOC}^{\min} \le \mathrm{SOC} \le \mathrm{SOC}^{\max};\ & P_{\mathrm{batt}}^{\min} \le P_{\mathrm{batt}} \le P_{\mathrm{batt}}^{\max} \\ \omega_{\mathrm{eng}}^{\min} \le \omega_{\mathrm{eng}} \le \omega_{\mathrm{eng}}^{\max};\ & T_{\mathrm{eng}}^{\min} \le T_{\mathrm{eng}} \le T_{\mathrm{eng}}^{\max} \\ T_{\mathrm{mot}}^{\min} \le T_{\mathrm{mot}} \le T_{\mathrm{mot}}^{\max};\ & \omega_{\mathrm{mot}}^{\min} \le \omega_{\mathrm{mot}} \le \omega_{\mathrm{mot}}^{\max} \\ T_{\mathrm{gen}}^{\min} \le T_{\mathrm{gen}} \le T_{\mathrm{gen}}^{\max};\ & \omega_{\mathrm{gen}}^{\min} \le \omega_{\mathrm{gen}} \le \omega_{\mathrm{gen}}^{\max} \end{aligned} \tag{9}$$

[1]The HEV has a conventional braking system in addition to the regenerative braking system. The braking power drained by the conventional brakes follows a different energy path, since it does not recharge the battery.

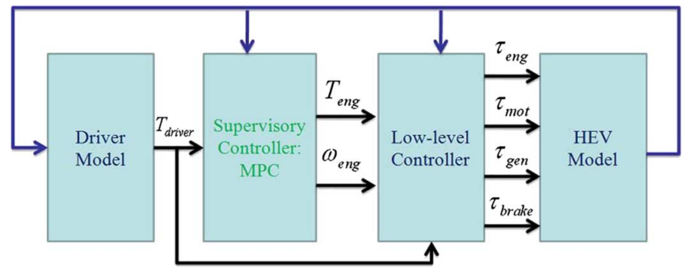

Fig. 2. Hierarchial control system.

where $\cdot^{\min}$ and $\cdot^{\max}$ denote the minimum and maximum bounds which may vary.

Based on the previous equations and assumptions, the control-oriented model can be represented by

$$\dot{x} = f(x, u, v) \quad y = g(x, u, v) \tag{10}$$

where

$$x = \mathrm{SOC} \quad u = \begin{bmatrix} T_{\mathrm{eng}} \\ \omega_{\mathrm{eng}} \end{bmatrix} \quad v = \begin{bmatrix} T_{\mathrm{driver}} \\ V \end{bmatrix} \quad y = \begin{bmatrix} \dot{m}_f \\ P_{\mathrm{batt}} \\ \omega_{\mathrm{gen}} \\ T_{\mathrm{mot}} \\ T_{\mathrm{gen}} \end{bmatrix}$$

x is the state, u is the control input, v is the measured disturbance, and y is the output of the model.

III. Control System Architecture

The objective of the energy management system is to minimize fuel consumption while ensuring that all the constraints are enforced. In this work, we manage the complexity of the problem by decomposing the controller into two levels. The first or supervisory level finds the optimum values for the two degrees of freedom of the system, engine speed and torque, at each sampling time. These optimal values are applied as the references to the second, low-level, controller where the engine, motor, generator, and friction brake torques are calculated. A block-diagram of the closed-loop model is shown in Fig. 2. In the low-level controller, standard control loops (PI controllers in PSAT) are used for reference tracking.

At the supervisory level, the energy management problem can be viewed as a constrained nonlinear dynamic optimization problem which is addressed here using model predictive control (MPC). The MPC controller calculates a future control sequence that minimizes a performance index which reflects the optimization goals subject to the equations of the dynamic model of the system and to the constraints. Then it applies the first element of the computed control sequence to the HEV model. The process is repeated at the next time step by moving the prediction horizon one step forward. Since the engine zero speed is a feasible MPC solution, a separate engine on/off strategy, as the one in PSAT controller [12], is not required. This research investigates two MPC methodologies developed based on two forms of cost functions which are discussed in the next sections.

IV. LTV-MPC Optimal Controller for the Power-Split HEV Energy Management

In the first methodology, a quadratic cost functional is chosen for the HEV fuel minimization problem and a LTV-MPC is employed to solve the problem online. The performance index is defined by

$$J = \int_{t}^{t+\Delta t} \left(w_f \cdot (\dot{m}_f(\tau))^2 + w_{\mathrm{SOC}} \cdot (\mathrm{SOC}(\tau) - \mathrm{SOC}_r)^2 \right) d\tau \tag{11}$$

where $\Delta t > 0$ is the prediction time horizon, and $w_f > 0$ and $w_{\mathrm{SOC}} > 0$ are the penalty weights. Based on the control-oriented model and the constraints in (9) and (10), the moving horizon optimal control problem at each time is defined by

$$\begin{aligned}
&\min_{\substack{u(\tau) \\ t \le \tau \le t+\Delta t}} \int_{t}^{t+\Delta t} \Big(w_f \cdot (\dot{m}_f(\tau))^2 \\
&\qquad\qquad + w_{\mathrm{SOC}} \cdot (\mathrm{SOC}(\tau) - \mathrm{SOC}_r)^2 \Big) d\tau \\
&\mathrm{SOC} = f\left(u(\tau), v(\tau)\right) \\
&\mathrm{SOC}_{\min} \le \mathrm{SOC}(\tau) \le \mathrm{SOC}_{\max},\ u(\tau) \in U,\ y(\tau) \in Y
\end{aligned} \tag{12}$$

where U and Y are the sets of admissible inputs and outputs according to (9). The quadratic finite-horizon optimal control problem (12) can be solved using LTV MPC approach as explained in the following sections.

A. Linear Model Predictive Control

The LTV-MPC control strategy is based on the standard MPC method for the linear systems which is briefly reviewed here. More details can be found in [19] and [20]. In the standard MPC, a finite-horizon quadratic cost functional penalizes deviation of the system output vector y from the corresponding reference vector r. In its more general form, the associated optimization problem can be formulated in discrete-time as

$$\begin{aligned}
\min_{\Delta U} J = \sum_{i=0}^{P-1} & \|u(k+i|k) - u_{target}(k)\|^2_{w_i^u} \\
& + \|\Delta u(k+i|k)\|^2_{w_i^{\Delta u}} \\
& + \|y(k+i+1|k) - r(k+i+1)\|^2_{w_{i+1}^y} + \rho_\varepsilon \varepsilon^2
\end{aligned}$$

subject to

$$\begin{aligned}
&\begin{cases} x(k+i+1|k) = Ax(k+i|k) + B_u u(k+i|k) \\ +B_v v(k+i|k) \\ y(k+i|k) = Cx(k+i|k) + D_v v(k+|k) \end{cases} \\
&u_i^{\min} \le u(k+i|k) \le u_i^{\max} \\
&\Delta u_i^{\min} \le \Delta u(k+i|k) \le \Delta u_i^{\max} \\
&-\varepsilon + y_i^{\min} \le y(k+i+1|k) \le y_i^{\max} + \varepsilon \\
&\Delta u(k+i|k) = 0 \text{ for } i = M, \ldots, P \\
&\varepsilon \ge 0
\end{aligned} \tag{13}$$

where P is the prediction horizon, M is the control horizon, $\Delta U = [\Delta u(k|k), \ldots, \Delta u(k+M-1|k)]^T$ is the sequence of input increments to be optimized, v is the vector of known inputs or measured disturbances, w_i^u, $w_i^{\Delta u}$, w_{i+1}^y, and ρ_ε are the weighting factors at the ith sample time, $x(k+i|k) \in R^n$ is the predicted state vector, $u(k+i|k) \in R^m$ is the vector of the manipulated variables, $y(k+i|k)$ is the vector of the predicted outputs, $r(k)$ is the vector of the output references, $u_{\mathrm{target}}(k)$ is the vector of the input steady-state references, and ε is the softening (slack) variable used to avoid infeasibility. Using the discrete model of the system, the outputs over a finite future horizon are predicted by

$$\begin{aligned}
y(k+i+1|k) = C\Bigg[& A^{i+1}x(k) + \sum_{l=0}^{i} A^i B_u \\
& \times \left(u(k-1) + \sum_{j=0}^{l} \Delta u(k+j|k) \right) \\
& + B_v v(k+l|k) \Bigg] + D_v v(k).
\end{aligned} \tag{14}$$

Substituting predicted trajectories of the outputs into the performance index J and output constraints, the optimization problem can be formulated as a quadratic program (QP) with linear inequality constraints

$$[\Delta U^*, \varepsilon] = \arg \min_{\Delta U, \varepsilon} \frac{1}{2} \Delta U^T H \Delta U + F^T \Delta U$$

subject to

$$G_u \Delta U + G_\varepsilon \varepsilon \le W \tag{15}$$

where H, F, G_u, G_ε, and W are constant matrices and functions of references, measured inputs, input targets, the last control input, and the measured or estimated states at current sample time [19], [20]. After solving QP problem (15) and obtaining the optimal input sequence ΔU^*, the control input to the plant is obtained by

$$u(k) = u(k-1) + \Delta u^*(k|k). \tag{16}$$

B. LTV-MPC Energy Management Strategy

In the LTV-MPC approach, the nonlinear prediction model (10) is linearized at each sample time around the current operating conditions and the linearized model is used to formulate the linear MPC problem (13). Then the control inputs are obtained by applying the linear MPC at that sample time. The stability and disturbance rejection properties for this approach are addressed in the literature as in [11], [21][22]. In the energy management based on the linear time-varying MPC, the following actions are performed at each sampling time (k).

- Measurement/estimation of system state $(\mathrm{SOC}(k))$.
- Prediction of the torque demand and vehicle speed (measured disturbance) over the prediction horizon. The future driver torque demand, which is usually unknown, is assumed to be exponentially decreasing over the prediction horizon [10]

$$T_{\mathrm{driver}}(k+i) = T_{\mathrm{driver}}(k) e^{\left(\frac{-i\tau_s}{\tau_d}\right)} \quad i = 1, 2, \cdots, P \tag{17}$$

  where $T_{\mathrm{driver}}(k)$ is the known value of the driver torque demand at the beginning of the prediction horizon, τ_s is the sample time and τ_d determines the decay rate. The effectiveness of (17) has been later confirmed by simulations.

By using the above driver torque model and by numerical integration of the vehicle speed dynamics (7) over the future time horizon, the future velocity profile is predicted.

- Linearization of the nonlinear model around the current operating conditions to obtain a linear system

$$\begin{cases} \dot{x} = \tilde{A}x + \tilde{B}_u u + \tilde{B}_v v + \tilde{F} \\ y = \tilde{C}x + \tilde{D}_u u + \tilde{D}_v v + \tilde{G} \end{cases} \quad (18)$$

where

$$\begin{aligned} \tilde{A} &= \left(\frac{\partial f}{\partial x}\right)_{(x_0,u_0,v_0)}; \quad \tilde{B}_u = \left(\frac{\partial f}{\partial u}\right)_{(x_0,u_0,v_0)} \\ \tilde{B}_v &= \left(\frac{\partial f}{\partial v}\right)_{(x_0,u_0,v_0)}; \quad \tilde{C} = \left(\frac{\partial g}{\partial x}\right)_{(x_0,u_0,v_0)} \\ \tilde{D}_u &= \left(\frac{\partial g}{\partial u}\right)_{(x_0,u_0,v_0)}; \quad \tilde{D}_v = \left(\frac{\partial g}{\partial v}\right)_{(x_0,u_0,v_0)} \\ \tilde{F} &= f(x_0,u_0,v_0) - \tilde{A}x_0 - \tilde{B}_u u_0 - \tilde{B}_v v_0 \\ \tilde{G} &= g(x_0,u_0,v_0) - \tilde{C}x_0 - \tilde{D}_u u_0 - \tilde{D}_v v_0 \end{aligned} \quad (19)$$

x_0, u_0, and v_0 are the current values of the state, input, and the measured disturbances to the system, respectively, and $g(x_0, u_0, v_0)$ is the vector of the current measurements of the outputs. In order to remove input-output direct feedthrough in accordance to the standard MPC formulation presented in Section IV-A, the linearized system is augmented with fast filters with time constant T_f, chosen to be at least 5–10 times faster than the fastest time constant of the plant. The augmented linearized system can be represented as

$$\begin{bmatrix} \dot{x} \\ \dot{x}_a \end{bmatrix} = \underbrace{\begin{bmatrix} 0_{1\times1} & \tilde{B}_u \\ 0_{3\times1} & -1/T_f I_{3\times3} \end{bmatrix}}_{A^c} \begin{bmatrix} x \\ x_a \end{bmatrix} + \underbrace{\begin{bmatrix} 0_{1\times3} \\ 1/T_f I_{3\times3} \end{bmatrix}}_{B_u^c} u + \underbrace{\begin{bmatrix} \tilde{B}_v & I_{1\times1} & 0_{1\times6} \\ 0_{3\times2} & 0_{3\times1} & 0_{3\times6} \end{bmatrix}}_{B_v^c} \begin{bmatrix} v \\ \tilde{F} \\ \tilde{G} \end{bmatrix}$$

$$[y] = \underbrace{[\tilde{C} \quad \tilde{D}_u]}_{C^c} \begin{bmatrix} x \\ x_a \end{bmatrix} + \underbrace{[\tilde{D}_v \quad 0_{6\times1} \quad I_{6\times6}]}_{D_v^c} \begin{bmatrix} v \\ \tilde{F} \\ \tilde{G} \end{bmatrix}. \quad (20)$$

- Time discretization of (20) with sampling period τ_s and application of the linear MPC (13) to the resulting model to compute the control input, as explained in Section IV-A.
- If the MPC requested power, $T_{\text{eng}} \times \omega_{\text{eng}}$, is greater than zero, the MPC decisions are applied to the plant; otherwise, the engine is turned off and T_{eng} and ω_{eng} are set to zero.

C. LTV-MPC Simulation Results and Discussion

The design parameters of the standard MPC are the penalty weights and prediction and control horizons. In addition, in this work, the time constant τ_d in the torque model (17) is another tuning parameter. These parameters are tuned via various simulations and observations over different driving conditions, some of which are presented in the next section. In the simulations, the sampling period of MPC is 1 s and the prediction and control horizons are chosen five steps. Also the performance index weights and the demanded torque time constant are chosen to be $w_{\text{SOC}} = 1$, $w_f = 50$, and $\tau_d = 1$ s. The fast filter time constant is $T_f = 0.01$ s. Before showing the simulation results over standard drive cycles, we discuss first a driving scenario that includes a 0 to 70 (km/hr) acceleration, a constant 70 (km/hr) cruise, and then deceleration to a stop which is useful to understand the different operating modes of the power-split HEV. The results are presented in Figs. 3 and 4.

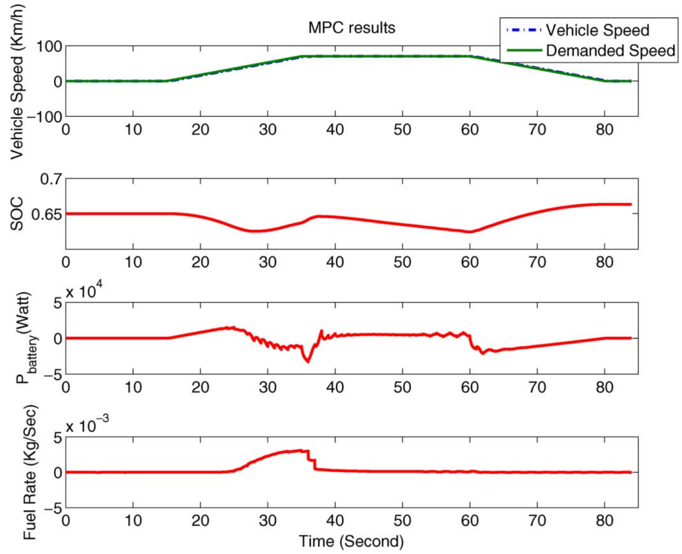

Fig. 3. LTV-MPC results with acceleration-cruise-brake cycle: vehicle speed, SOC, battery power, and fuel rate.

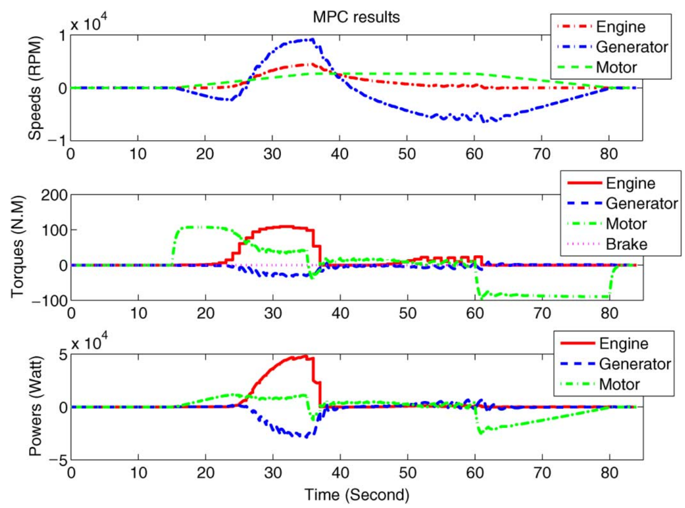

Fig. 4. LTV-MPC results with acceleration-cruise-brake cycle: engine, generator, and motor's speed, torque, and power.

As seen in Fig. 4, during acceleration (15 to 35 s), the motor provides the initial torque before the engine is engaged and then it continues to assist the engine. The generator provides negative or reaction torque to transmit the engine torque to the wheels. This operation is called the positive-split [18]. Later, during cruise (35 to 60 s), the controller reduces the generator speed to negative values and the generator operates in motoring mode.

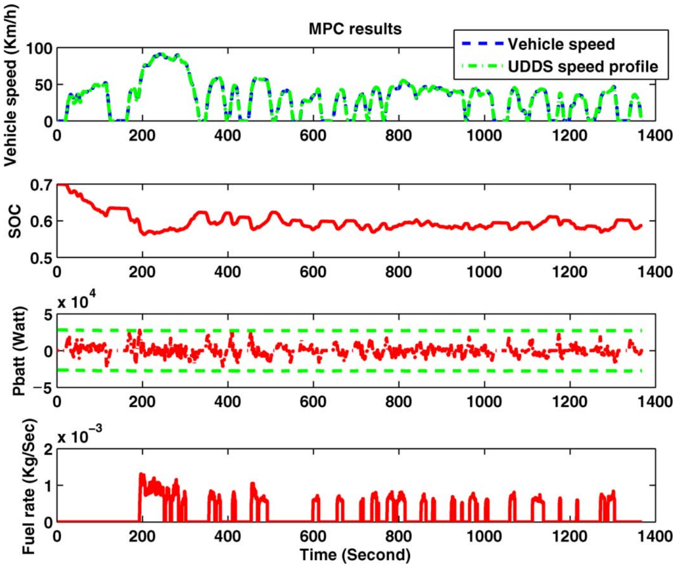

Fig. 5. LTV-MPC on UDDS cycle: velocity, SOC, battery power, and fuel rate (time intervals with zero fuel rate correspond to engine being shut down).

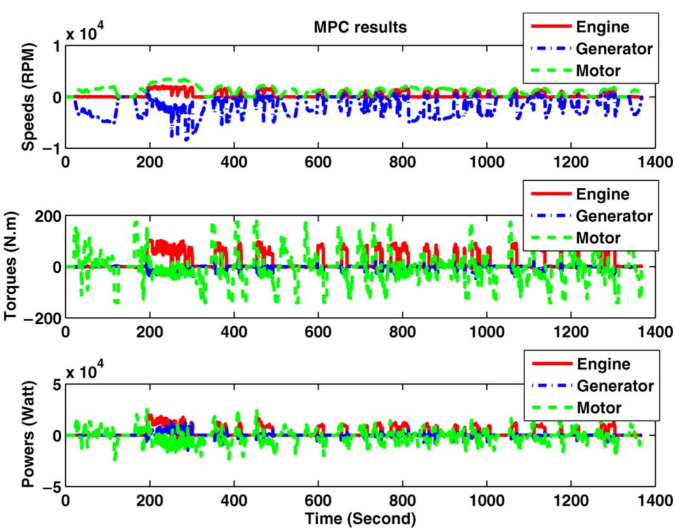

Fig. 6. LTV-MPC on UDDS cycle: engine, generator, and motor speeds, torques, and powers.

Since during cruise, the vehicle speed is relatively high but the power demand is relatively low; the negative generator speed reduces the engine speed according to (5) and (6). This HEV operation mode is called the negative-split [18]. During deceleration, the motor operates in the generating mode and energy is recuperated into the battery. This mode is called the regenerative braking mode. The ripples in the battery power and fuel consumption rate plots are due to the discrete-time MPC updates.

To demonstrate the LTV-MPC strategy performance quantitatively, we ran simulations over standard city and highway driving cycles over the detailed HEV model extracted from PSAT. At each sample time, the MPC constraints are updated based on the feedback from the plant model. The target SOC is set to 0.7 which is the default value in PSAT for this HEV. The upper and lower limits of SOC are set to 0.2 and 0.9,

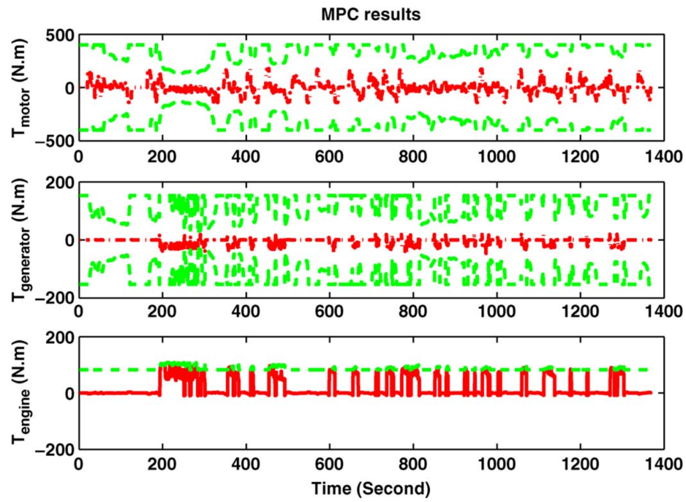

Fig. 7. LTV-MPC on UDDS cycle: engine, generator, and motor torques and constraints.

respectively. Other constraints are updated as functions of operating points based on the online feedback from the PSAT model. The MPC prediction model and tuning parameters are kept unchanged as described before. The MPC controller issues its optimal evaluation of engine torque and speed which are passed to the lower level controller. Figs. 5–7 show simulation results over urban dynamometer driving schedule (UDDS) cycle. The dashed lines indicate the constraints on the different physical outputs. It can be observed that the LTV-MPC controller enforces all of the constraints over the cycle. The MPC performance is also tested on a highway driving scenario, the highway fuel economy driving schedule (HWFET) cycle, and the same performance is observed. Table II compares the fuel economy and the initial and final battery state of charge for both MPC and PSAT controllers ran on the same PSAT model of the HEV. In order to remove the effect of different initial and final SOCs on the fuel economy, we ran the simulations over the same cycle multiple times until the system reaches a charge balance. The fuel economy values with equal initial and final SOCs are also presented in Table II. It is observed that the LTV-MPC fuel economy results are comparable with those of PSAT. Regardless of the fact that the developed LTV-MPC strategy is a systematic optimal control method to solve the fuel minimization problem, the fuel economy values over the standard drive cycles are not improved with respect to the ones of the available rule-based controller of PSAT. We attribute this to the model error introduced by linearization of the control-oriented model. Furthermore, the feasible reference for the fuel consumption rate cannot be zero most of the time. Because of these issues, we observed that even increasing the prediction and control horizons of the LTV-MPC with the current quadratic cost functional cannot noticeably improve the fuel economy. Basing on the previous experience of [23] where better results obtained by using a piecewise linear approximation of the fuel consumption map for an ERAD HEV configuration that allows better prediction, yet it results in a hybrid MPC approach requiring solution of mixed-integer programs. In the next sections, we develop a nonlinear MPC

TABLE I
LTV-MPC AND PSAT RESULTS

Controller	*Initial SOC*	*Final SOC*	*FuelEconomy (mpg)*
UDDS cycle			
Controller	*Initial SOC*	*Final SOC*	*FuelEconomy (mpg)*
LTV-MPC	0.70	0.59	84.31
	0.59	0.59	73.02
PSAT	0.70	0.67	78.55
	0.67	0.67	76.03
Highway FET cycle			
Controller	*Initial SOC*	*Final SOC*	*FuelEconomy (mpg)*
LTV-MPC	0.70	0.63	70.1
	0.63	0.63	66.12
PSAT	0.70	0.64	69.43
	0.63	0.63	65.52

TABLE II
MPC AND PSAT RESULTS (CYCLES FROM [12])

Controller	*Initial SOC*	*Final SOC*	*FuelEconomy (mpg)*
UDDS cycle			
Controller	*Initial SOC*	*Final SOC*	*FuelEconomy (mpg)*
LTV-MPC	0.70	0.59	84.31
	0.59	0.59	73.02
PSAT	0.70	0.67	78.55
	0.67	0.67	76.03
NMPC	0.70	0.68	82.37
	0.68	0.68	80.1
Highway FET cycle			
Controller	*Initial SOC*	*Final SOC*	*FuelEconomy (mpg)*
LTV-MPC	0.70	0.63	70.1
	0.63	0.63	66.12
PSAT	0.70	0.64	69.43
	0.63	0.63	65.52
NMPC	0.70	0.74	69.63
	0.74	0.74	72.2

approach that does not require linearizations and uses a different cost function.

V. NONLINEAR MPC FOR POWER-SPLIT HEV ENERGY MANAGEMENT

In the second methodology, a different cost function is defined for the fuel minimization problem. It will be shown that with this choice of cost function and application of nonlinear MPC the fuel economy is improved versus both LTV-MPC and PSAT controllers. The total fuel cost over an entire cycle which starts at time t_0 and ends at time t_f can be obtained by

$$J = \int_{t_0}^{t_f} \dot{m}_f\left(u(t)\right) dt + h\left(\mathrm{SOC}(t_f)\right) \tag{21}$$

where $h(\mathrm{SOC}(t_f))$ penalizes the deviation of SOC at the end of the cycle from a reference value, SOC_r. As was previously discussed in Section IV, the objective of the energy management strategy is to minimize a cost function [here (21)] while satisfying the dynamical equations (10) and the constraints (9). However in real applications, the driving conditions over long time horizons are not generally known in advance and furthermore, the parameters of the model and of the constraints may vary. Moreover, the solution of the optimal control problem over a long horizon is computationally demanding. To address these issues, we propose to use Bellman's principle of optimality [13] to split the above optimal control problem into an integrated stage cost and an approximated minimum fuel cost from the end of the prediction horizon to the end of the drive cycle. We then propose to solve the problem using the receding horizon framework. At time $t \leq t_f$, the cost function is

$$J\left(u, \mathrm{SOC}(t), t\right) = \int_{t}^{t_f} \dot{m}_f\left(u(\tau)\right) d\tau + h\left(\mathrm{SOC}(t_f)\right) \tag{22}$$

where $\mathrm{SOC}(t)$ is any admissible state value at time t. The performance metric depends on the values[2] of $\mathrm{SOC}(t)$, t, and the control inputs over the interval $[t, t_f]$. The minimum cost or cost-to-go is obtained by

$$J^*\left(\mathrm{SOC}(t), t\right) = \min_{\substack{u(\tau)\\ t\leq\tau\leq t_f}} \left\{ \int_{t}^{t_f} \dot{m}_f\left(u(\tau)\right) d\tau + h\left(\mathrm{SOC}(t_f)\right) \right\} \tag{23}$$

subject to the constraints (9) and dynamics (10). By dividing the time interval $[t, t_f]$ one can write

$$\begin{aligned} J^*\left(\mathrm{SOC}(t), t\right) = \min_{\substack{u(\tau)\\ t\leq\tau\leq t_f}} & \left\{ \int_{t}^{t+\Delta t} \dot{m}_f\left(u(\tau)\right) d\tau \right. \\ & \left. + \int_{t+\Delta t}^{t_f} \dot{m}_f\left(u(\tau)\right) d\tau + h\left(\mathrm{SOC}(t_f)\right) \right\} \end{aligned} \tag{24}$$

where Δt is a chosen time horizon. Bellman's principle of optimality implies that

$$\begin{aligned} J^*\left(\mathrm{SOC}(t), t\right) = \min_{\substack{u(\tau)\\ t\leq\tau\leq t+\Delta t}} & \left\{ \int_{t}^{t+\Delta t} \dot{m}_f\left(u(\tau)\right) d\tau \right. \\ & \left. + J^*\left(\mathrm{SOC}(t+\Delta t), t+\Delta t\right) \right\}. \end{aligned} \tag{25}$$

The minimum fuel cost over the interval $[t+\Delta t, t_f]$, i.e., $J^*(\mathrm{SOC}(t+\Delta t), t+\Delta t)$, is not in general a known function of SOC. In the next section, we show how this function can be approximated, hence enabling us to solve the above fuel minimization problem using a receding horizon approach.

A. Approximation of the Fuel Cost-to-Go Function

In this section, we derive an approximation for the minimum fuel cost as a function of the battery's state of charge. An approximation of the cost-to-go will be sufficient because the optimal solutions are recalculated in a receding horizon manner at each time step. Assuming that a Taylor series expansion of $J^*(\mathrm{SOC}(t+\Delta t), t+\Delta t)$ around $\mathrm{SOC}^*(t+\Delta t)$ can be made, we obtain

$$\begin{aligned} & J^*\left(\mathrm{SOC}(t+\Delta t), t+\Delta t\right) \\ & \quad = J^*\left(\mathrm{SOC}^*(t+\Delta t), t+\Delta t\right) \\ & \qquad + \frac{\partial J^*}{\partial \mathrm{SOC}}\left(\mathrm{SOC}^*(t+\Delta t), t+\Delta t\right) \cdot \Delta\mathrm{SOC} \\ & \qquad + O(\Delta\mathrm{SOC}^2) \end{aligned} \tag{26}$$

[2]Note that the SOC is the only dynamical state of the system. This explain the variables in the cost-to-go in (22).

This article has been accepted for inclusion in a future issue of this journal. Content is final as presented, with the exception of pagination.

where $\Delta\text{SOC} = (\text{SOC}(t+\Delta t) - \text{SOC}^*(t+\Delta t))$. As shown in Appendix A, by observing the relationship between the Pontryagin's minimum principle and HJB equations as represented in [13], if SOC^* denotes the optimal trajectory from current time t and initial state $\text{SOC}(t)$ to the end of the trip, we can rewrite (26) as

$$\begin{aligned} J^*(\text{SOC}(t+\Delta t), t+\Delta t) &\cong J^*(\text{SOC}^*(t+\Delta t), t+\Delta t) \\ &+\lambda(\text{SOC}(t),t)\cdot(\text{SOC}(t+\Delta t) - \text{SOC}^*(t+\Delta t)) \end{aligned} \tag{27}$$

where

$$\lambda(\text{SOC}(t),t) = \frac{\partial J^*}{\partial \text{SOC}}(\text{SOC}(t),t). \tag{28}$$

By adding and subtracting the constant reference value SOC_r, to and from the last term of (27) we obtain

$$\begin{aligned} J^*(\text{SOC}(t+\Delta t), t+\Delta t) &\cong \alpha(\text{SOC}(t),t) \\ &+\lambda(\text{SOC}(t),t)\cdot(\text{SOC}(t+\Delta t) - \text{SOC}_r) \end{aligned} \tag{29}$$

where $\alpha(\text{SOC}(t),t)$ is

$$\begin{aligned} \alpha = {} & J^*(\text{SOC}^*(t+\Delta t), t+\Delta t) \\ &+\lambda(\text{SOC}(t),t)\cdot(\text{SOC}_r - \text{SOC}^*(t+\Delta t)). \end{aligned} \tag{30}$$

Substituting (29) into cost function (25) we get

$$\begin{aligned} & J^*(\text{SOC}(t),t) \\ &= \min_{\substack{u(\tau) \\ t\le\tau\le t+\Delta t}} \Bigg\{ \alpha(\text{SOC}(t),t) + \int_t^{t+\Delta t} \dot{m}_f(u(\tau))\,d\tau \\ &\qquad + \lambda(\text{SOC}(t),t) \\ &\qquad \cdot (\text{SOC}(t+\Delta t) - \text{SOC}_r) \Bigg\}. \end{aligned} \tag{31}$$

Since α in (31) is not a function of the control inputs, it does not affect the selection of the optimal control. Therefore the optimal control over the interval $[t, t+\Delta t]$ is obtained by solving the following finite-time optimal control problem:

$$\begin{aligned} & \min_{\substack{u(\tau) \\ t\le\tau\le t+\Delta t}} \int_t^{t+\Delta t} \dot{m}_f(\tau)d\tau + \lambda(\text{SOC}(t),t) \\ & \quad \cdot (\text{SOC}(t+\Delta t) - \text{SOC}_r) \\ & \dot{\text{SOC}} = f(u(\tau), v(\tau)) \\ & \text{SOC}_{\min} \le \text{SOC}(\tau) \le \text{SOC}_{\max}, u(\tau) \in U, y(\tau) \in Y \end{aligned} \tag{32}$$

where U and Y are the sets of admissible inputs and outputs according to (9). Note that SOC at time t in (32) is the measured value of the state at the current time and is known. We will solve this finite-horizon optimal control problem in a receding horizon manner as explained in the next section.

As shown in Appendices A and B, the parameter λ is related to both the equivalent factor in the ECMS method and the rate of change of minimum cost with respect to the SOC. An admissible range for λ can be obtained as explained in the ECMS literature [24] or from the DP solutions over different driving cycles [14]. In what follows, it is shown that λ can be approximated by a tunable piecewise linear function over the admissible range. Using (28) and assuming sufficient smoothness of J^*, the Taylor series expansion of the function λ around the SOC_r yields

$$\begin{aligned} \lambda(\text{SOC}(t),t) = {} & \frac{\partial J^*}{\partial \text{SOC}}(\text{SOC}_r,t) + \frac{\partial^2 J^*}{\partial \text{SOC}^2}(\text{SOC}_r,t) \\ & \times (\text{SOC}(t) - \text{SOC}_r) + O\left(\Delta\text{SOC}_r^2\right) \end{aligned} \tag{33}$$

where $\Delta\text{SOC}_r = (\text{SOC}(t) - \text{SOC}_r) < 0.5$. By defining $\lambda_0 = (\partial J^*/\partial\text{SOC})(\text{SOC}_r,t)$ and $\mu = (\partial^2 J^*/\partial\text{SOC}^2)(\text{SOC}_r,t)$ as two tuning design parameters and ignoring the higher order terms we obtain

$$\lambda(\text{SOC}(t),t) \cong \lambda_0 + \mu\Delta\text{SOC}_r \tag{34}$$

which approximates λ as an affine function of the state.

B. Nonlinear MPC (NMPC) Energy Management

The optimal control problem in (32) is first discretized with a sample time τ_s and then is solved using dynamic programming. More specifically, the following actions are performed at each sampling time (k).

- The constraints are updated using the feedback from the HEV model.
- The future torque demand and vehicle speed (measured disturbances), unknown over the prediction horizon, are initialized at the current value and predicted according to (17) and (7).
- As explained in Section V-A, the parameter λ is calculated according to (34).
- Using dynamic programming, the updated MPC problem (32) is solved numerically over the (short) prediction horizon. Since the MPC prediction horizon is usually short compared to the whole drive cycle, the computations can be done in real-time.
- Consistent with standard MPC framework, the first input in the sequence of the calculated optimal inputs over the prediction horizon is applied to the plant if the MPC requested power, $T_{\text{eng}} \times \omega_{\text{eng}}$, is greater than zero; otherwise the engine is turned off and T_{eng} and ω_{eng} are set to zero.

The above steps are repeated by receding the prediction horizon one step forward. Repeating these calculations for every new measurement yields a state feedback control law.[3]

C. NMPC Simulation Results and Discussion

To quantitatively demonstrate the validity of the NMPC strategy, we ran simulations over different driving cycles with the same parameters and HEV model of LTV-MPC presented in Section IV-C. Some of the results are presented in Fig. 8 and in Table II.

The table compares the fuel economy and the initial and final SOCs of the LTV-MPC controller, the base controller of PSAT,

[3]Note that an intermediate solution where linear time varying dynamics are used with the cost function (32) can also be considered. However, this approach may not, in general, achieve the same performance as NMPC due to the mismatch in prediction caused by the linearization of the dynamics and of the fuel flow equation. Due to limited space, this intermediate approach is not further discussed here.

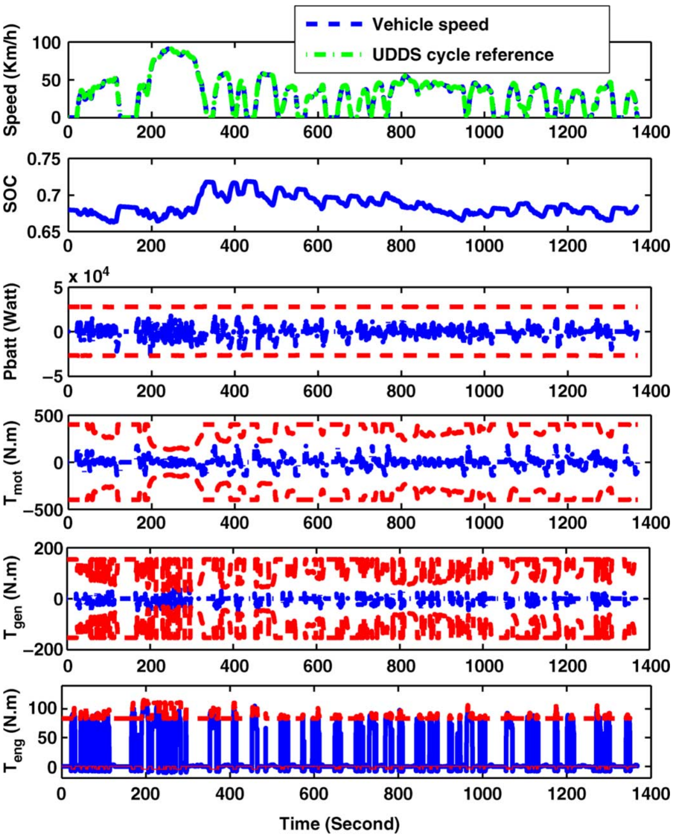

Fig. 8. Outputs and constraints of the NMPC closed-loop model over the UDDS cycle.

and the nonlinear MPC (NMPC) controller. In order to remove the effect of different initial and final SOCs on the fuel economy, we ran the simulations over the same cycle multiple times until the system reached a charge balance (i.e., $\mathrm{SOC}(0) = \mathrm{SOC}(t_f)$). The fuel economy values with equal initial and final SOCs are used to compare the performance of different controllers. It can be observed that over both city and highway driving cycles, the NMPC controller achieves an improved fuel economy. Also in Table III, the closed-loop model is simulated over other drive cycles and it can be observed that the NMPC strategy consistently shows better fuel economy, achieved by using the same control model and tuning parameters in all of the simulations. We should mention here that the computational time of the nonlinear MPC approach is about two times larger than the LTV-MPC. However, the nonlinear MPC uses a DP code written in MATLAB script and is not necessarily optimized for computations. On the other hand, the LTV-MPC uses the MATLAB MPC toolbox [25] which has a C code to solve MPC. Furthermore, because the (nonlinear) control-oriented model has differences with the full-order plant model, conditions that guarantee constraint satisfaction of the nonlinear MPC (as well as the LTV-MPC) in the closed-loop model remain open for further investigation. However, state constraints can be implemented as soft constraints to avoid infeasibility.

TABLE III
MPC AND PSAT RESULTS (CYCLES FROM [12])

Controller	*Initial SOC*	*Final SOC*	*FuelEconomy (mpg)*
US06 cycle			
PSAT	0.70	0.62	45.4
	0.6	0.6	42.8
NMPC	0.70	0.69	42.49
	0.69	0.69	46.01
SC03 cycle			
PSAT	0.70	0.68	71.29
	0.68	0.68	69
NMPC	0.70	0.69	76.66
	0.69	0.69	74.77
JC08 cycle			
PSAT	0.70	0.67	85.67
	0.67	0.67	81
NMPC	0.70	0.71	82
	0.71	0.71	83.6
NY City cycle			
PSAT	0.70	0.66	68.68
	0.64	0.64	52.6
NMPC	0.70	0.67	66.47
	0.67	0.67	58.25

VI. CONCLUSION

Two MPC-based methodologies have been developed for solving the fuel minimization problem of the power-split hybrid electric vehicles. In the first methodology, a quadratic cost function is defined for the HEV optimal control problem and a linear time-varying MPC is employed to solve the problem online. In order to improve the fuel economy, a second cost function is introduced by dividing the fuel consumption cost into a stage cost and an approximation of cost-to-go as a function of battery's state of charge. The short-horizon allows to solve the fuel minimization problem online in a nonlinear MPC framework. The proposed methods are systematic in both design and tuning and predictive in nature. The results over a PSAT closed-loop model of a power-split HEV show that with the nonlinear MPC approach, the fuel economy is improved noticeably with respect to that of an available controller in the commercial PSAT software and compared to the linear time-varying MPC controller.

APPENDIX A
MINIMUM PRINCIPLE AND HEV FUEL MINIMIZATION

The necessary conditions for the optimality can be obtained by applying the variational approach (Pontryagin minimum principle as in [13]) to the fuel minimization problem. The Hamiltonian for problem (21) is defined as

$$H\left(\mathrm{SOC}(\tau), u(\tau), p(\tau), \tau\right) = \dot{m}_f\left(u(\tau)\right) + p(\tau)\left[f\left(u(\tau), \tau\right)\right] \tag{35}$$

where $\tau \in [t, t_f]$. Using this notation, the necessary conditions for the optimality from current time t and an initial value of $\mathrm{SOC}(t)$ to the end of the drive cycle are

$$\begin{aligned} &H = \dot{m}_f\left(u(\tau)\right) + p(\tau)\left[f\left(u(\tau),\tau\right)\right] = H\left(u(\tau),p(\tau),\tau\right) \\ &\dot{\mathrm{SOC}}^*(\tau) = \frac{\partial H}{\partial p}\left(u^*(\tau),p^*(\tau),\tau\right) \\ &\dot{p}^*(\tau) = -\frac{\partial H}{\partial \mathrm{SOC}}\left(u^*(\tau),p^*(\tau),\tau\right) = 0 \\ &H\left(\mathrm{SOC}^*(\tau),u^*(\tau),p^*(\tau),\tau\right) \\ &\quad \le H\left(\mathrm{SOC}^*(\tau),u(\tau),p^*(\tau),\tau\right). \end{aligned} \tag{36}$$

Conditions (36) need to be satisfied for all admissible $u(\tau)$ in $t \le \tau \le t_f$. As it can be observed in (36), since f does not depend on SOC, $\partial H/\partial\mathrm{SOC} = 0$ and consequently we can write $p^*(\tau) = \lambda(\mathrm{SOC}(t),t)$. The relationship between HJB equations and the minimum principle [13] implies that

$$\begin{aligned} p^*(\tau) &= \frac{\partial J^*\left(\mathrm{SOC}^*(\tau),\tau\right)}{\partial\mathrm{SOC}} = \frac{\partial J^*\left(\mathrm{SOC}(t),t\right)}{\partial\mathrm{SOC}} \\ &= \lambda\left(\mathrm{SOC}(t),t\right). \end{aligned} \tag{37}$$

Thus for an initial time t and a state of the charge $\mathrm{SOC}(t)$ by replacing $\tau = t + \Delta t$

$$\frac{\partial J^*}{\partial\mathrm{SOC}}\left(\mathrm{SOC}^*(t+\Delta t),t+\Delta t\right) = \frac{\partial J^*}{\partial\mathrm{SOC}}\left(\mathrm{SOC}(t),t\right) \tag{38}$$

where $(\partial J^*/\partial\mathrm{SOC})(\mathrm{SOC}(t),t) = \lambda(\mathrm{SOC}(t),t)$. Note that $\mathrm{SOC}^*(\tau)$ is derived by relaxing its constraints (enforced online by MPC along the finite prediction horizon).

Appendix B
Parameter of the MPC Cost Functional and the ECMS Factor

In the ECMS method, an instantaneous cost function is defined by [4], [26]

$$J = \dot{m}_f(t) + S\cdot\frac{P\mathrm{batt}(t)}{H_f} \tag{39}$$

where S is the ECMS factor. The Hamiltonian calculated in Appendix A is

$$H = \dot{m}_f\left(u(t)\right) + p(t)\dot{\mathrm{SOC}}(t). \tag{40}$$

According to the Pontryagin's Minimum Principle [13]

$$J = H\left(\mathrm{SOC}(t),u(t),p^*(t),t\right) = \dot{m}_f\left(u(t)\right) + p^*(t)\dot{\mathrm{SOC}}(t). \tag{41}$$

By considering the dynamics of the battery and ignoring the power losses due to the internal resistance

$$\dot{\mathrm{SOC}}(t) \cong -\frac{P_{\mathrm{batt}}}{C_{\mathrm{batt}}V_{oc}}. \tag{42}$$

Hence it follows that

$$p^*(t) = \left(\frac{C_{\mathrm{batt}}V_{oc}}{H_f}\right)\cdot S. \tag{43}$$

From the relationship between HJB equation and the minimum principle as in [13], it follows that:

$$\lambda\left(\mathrm{SOC}(t),t\right) = p^*(t) = \left(\frac{C_{\mathrm{batt}}V_{oc}}{H_f}\right)\cdot S. \tag{44}$$

Acknowledgment

The authors would like to thank Dr. C. Zhang of Clemson University for his discussions in implementing the dynamic programming.

References

[1] M. Ehsani, Y. Gao, S. E. Gay, and A. Emadi, *Modern Electric, Hybrid Electric, and Fuel Cell Vehicles: Fundamentals, Theory, and Design*. Boca Raton, FL: CRC, 2004.
[2] C. Lin, H. Peng, J. W. Grizzle, and J. Kang, "Power management strategy for a parallel hybrid electric truck," *IEEE Trans. Control Syst. Technol.*, vol. 11, no. 6, pp. 839–849, Nov. 2003.
[3] C. Lin, H. Peng, and J. W. Grizzle, "A stochastic control strategy for hybrid electric vehicles," in *Proc. Amer. Control Conf.*, 2004, pp. 4710–4715.
[4] G. Paganelli, S. Delprat, T. M. Guerra, J. Rimaux, and J. J. Santin, "Equivalent consumption minimization strategy for parallel hybrid powertrains," in *Proc. Veh. Technol. Conf.*, 2002, pp. 2076–2081.
[5] C. Musardo, G. Rizzoni, and B. Staccia, "A-ECMS: An adaptive algorithm for hybrid electric vehicle energy management," in *Proc. IEEE Conf. Decision Control*, 2005, pp. 1816–1823.
[6] P. Pisu and G. Rizzoni, "A comparative study of supervisory control strategies for hybrid electric vehicles," *IEEE Trans. Control Syst. Technol.*, vol. 15, no. 3, pp. 506–518, May 2007.
[7] A. Sciarretta and L. Guzzella, "Control of hybrid electric vehicles," *IEEE Control Syst. Mag.*, vol. 27, no. 2, pp. 60–70, Feb. 2007.
[8] A. Sciarretta and L. Guzzella, "Control of hybrid electric vehicles," *IEEE Control System Magazine*, vol. 27, no. 4, pp. 60–67, Apr. 2007.
[9] G. Paganelli, S. Delprat, T. M. Guerra, J. Rimaux, and J. J. Santin, "Equivalent consumption minimization strategy for parallel hybrid powertrains," in *Proc. Veh. Technol. Conf.*, 2002, pp. 2076–2081.
[10] H. Borhan, A. Vahidi, A. Phillips, M. Kuang, and I. Kolmanovsky, "Predictive energy management of a power-split hybrid electric vehicle," in *Proc. Amer. Control Conf.*, 2009, pp. 3970–3976.
[11] P. Falcone, F. Borrelli, H. E. Tseng, J. Asgari, and D. Hrovat, "Linear time-varying model predictive control and its application to active steering systems: Stability analysis and experimental validation," *Int. J. Robust Nonlinear Control*, vol. 18, no. 8, pp. 1172–1177, 2004.
[12] Argonne National Laboratory, DuPage County, IL, "Powertrain system analysis toolkit (PSAT) documentation," 1946.
[13] D. E. Kirk, *Optimal Control Theory: An Introduction*. New York: Dover, 2004.
[14] L. Johannesson, S. Pettersson, and B. Egardt, "Predictive energy management of a 4QT series-parallel hybrid electric bus," *Control Eng. Practice*, vol. 17, pp. 1440–1453, 2009.
[15] G. Zini, J. Kern, J. , and M. Duoba, "Honda insight validation using PSAT," SAE, Warrendale, PA, Paper 2001-01-2538, 2001.
[16] A. Rousseau, J. Kwon, P. Sharer, S. Pagerit, and M. Duoba, "Integrating data, performing quality assurance, and validating the vehicle model for the 2004 Prius using PSAT," SAE, Warrendale, PA, Paper 2006-01-0667, 2006.
[17] J. Liu and H. Peng, "Modeling and control of a power-split hybrid vehicle," *IEEE Trans. Control Syst. Technol.*, vol. 16, no. 6, pp. 1242–1251, Nov. 2008.
[18] F. U. Syed, M. L. Kuang, J. Czubay, and H. Ying, "Derivation and experimental validation of a power-split hybrid electric vehicle model," *IEEE Trans. Control Syst. Technol.*, vol. 54, no. 6, pp. 1731–1747, Nov. 2006.
[19] J. M. Maciejowski*, Predictive Control With Constraints*. Englewood Cliffs, NJ: Prentice-Hall, 2002.
[20] G. C. Goodwin, M. Seron, and J. A. Dona*, Constrained Control and Estimation*. New York: Springer, 2005.
[21] Z. Wan and M. V. Kothare, "Efficient scheduled stabilizing output feedback model predictive control for constrained nonlinear systems," *IEEE Trans. Autom. Control*, vol. 49, no. 7, pp. 862–875, Jul. 2004.
[22] J. H. Lee and N. L. Ricker, "Extended Kalman filter based nonlinear model predictive control," *Ind. Eng. Chem. Res.*, vol. 33, no. 6, pp. 1530–1541, 1994.
[23] G. Ripaccioli, A. Bemporad, F. Assadian, C. Dextreit, S. Di Cairano, and I. V. Kolmanovsky, "Hybrid modeling, identification, and predictive control: An application to hybrid electric vehicle energy management," *Lecture Notes in Comput. Sci.*, vol. 5469, pp. 321–335, 2009.
[24] L. Guzzella and A. Sciarretta*, Vehicle Propusion Systems: Introduction to Modeling and Optimization*. New York: Springer, 2005, pp. 190–203.

[25] The MathWorks, Natick, MA, "Model predictive control toolbox," 2009.

[26] L. Serrao, S. Onori, and G. Rizzoni, "ECMS as a realization of Pontryagin's minimum principle for HEV control," in *Proc. Amer. Control Conf. (ACC)*, 2009, pp. 3964–3969.

Hoseinali Borhan (S'10) received the B.S. degree in mechanical engineering from the University of Tehran, Tehran, Iran, in 2000, and the M.S. degree in mechanical engineering from Sharif University of Technology, Tehran, Iran, in 2003. He is currently pursuing the Ph.D. degree in mechanical engineering from Clemson University, Clemson, SC.

In 2010, he was a visiting researcher with the Research and Advanced Engineering Center, Ford Motor Company, Dearborn, MI. Since 2010, he has been a visiting researcher with the University of Texas at Dallas. His current research focuses on the application of model predictive control in the optimal energy/power management of hybrid systems including hybrid electric powertrains and wind farms with battery storage systems.

Ardalan Vahidi (M'06) received the B.S. and M.S. degrees in civil engineering from Sharif University, Tehran, Iran, in 1996 and 1998, respectively, the M.S. degree in transportation safety from George Washington University, Washington, DC, in 2002, and the Ph.D. degree in mechanical engineering from the University of Michigan, Ann Arbor, in 2005.

He is currently an Assistant Professor with the Department of Mechanical Engineering, Clemson University, Clemson, SC. His current research interests include optimization-based control methods and control of vehicular and energy systems.

Anthony M. Phillips received the B.A. degree in physics from Gustavus Adolphus College, St. Peter, MN, in 1990 and the M.S. and Ph.D. degrees in mechanical engineering/control systems from the University of California, Berkeley, in 1993 and 1995, respectively.

Upon completing his study, he joined Ford Motor Company, Dearborn, MI, as a Product Development Engineer. He was appointed Technical Expert when he joined the Research and Advanced Engineering staff in 1998. In his current position as a Senior Technical Leader, he has responsibility for Ford's advanced vehicle control system development for all electrified vehicle applications. His research interests include vehicle energy management, distributed system control and control system development tools and methods. He holds 32 U.S. and international patents in automotive controls.

Dr. Phillips is a member of the Society of Automotive Engineers, the American Society of Mechanical Engineers, and the Editorial Board for the *International Journal of Alternative Propulsion*.

Ming L. Kuang received the M.S. degree in mechanical engineering from University of California, Davis, and the B.S. degree in mechanical engineering from South China University of Technology, People's Republic of China.

He is currently a Technical Leader in vehicle controls, Research and Advanced Engineering, Ford Motor Company, Dearborn, MI, leading the development of global vehicle control architecture and advanced hybrid vehicle controls. He has worked in both research and product development organizations in the area of vehicle dynamics and controls, electric and hybrid electric vehicles technology, and vehicle controls since 1991. In his prior position, he, as a Technical Expert, played an instrumental role in the development of hybrid vehicle controls and the successful launch of the first Escape Hybrid. He has authored and coauthored 30 technical papers published in IEEE journal and other engineering conferences. He holds 37 U.S. patents and 11 international patents.

Mr. Kuang was a recipient of major awards from both internal and external of Ford Motor Company.

Ilya V. Kolmanovsky (F'07) has received the M.S. and Ph.D. degrees in aerospace engineering and the M.A. degree in mathematics from the University of Michigan, Ann Arbor, in 1993, 1995, and 1995, respectively.

Before becoming a Professor with the Department of Aerospace Engineering, University of Michigan, in 2010, he was with Ford Motor Company, Dearborn, MI, for close to 15 years. He has published over 200 refereed journal and conference articles on a spectrum of theoretical topics, and on a variety of automotive and aerospace control applications. He is named as an inventor on 82 U.S. patents.

Dr. Kolmanovsky was a recipient of several awards, including the Donald P. Eckman Award of American Automatic Control Council, the IEEE Transactions on Control Systems Technology Outstanding Paper Award, and several innovation and technical achievement awards at Ford Motor Company. He is a member of IEEE Control Systems Society Board of Governors.

Stefano Di Cairano (M'08) received the Master's degree in computer engineering and the Ph.D. degree in information engineering from the University of Siena, Siena, Italy, in 2004 and 2008, respectively.

In 2008, he was granted the International Curriculum Option for Doctoral Studies in Hybrid Control for Complex Distributed and Heterogeneous Embedded Systems. In 2002–2003, he was a visiting student with the Technical University of Denmark, Lyngby, Denmark. In 2006–2007, he was a visiting researcher with the Control and Dynamical Systems Department, the California Institute of Technology, Pasadena, where he joined the team competing in the 2007 DARPA Urban Challenge. In 2008, he joined Powertrain Control Research and Advanced Engineering Department, Ford Motor Company, Dearborn, MI, where he is currently a Technical Expert. His research focuses on the application of optimization-based control algorithms to complex systems including powertrain, vehicle dynamics, energy management, and supply chains. His interests include automotive control, model predictive control, networked distributed control systems, hybrid systems, optimization algorithms, and stochastic control.